

# Spectroscopy with Multi-Hadron Interpolating Operators in Lattice Quantum Chromodynamics

Adrian Leigh Kiratidis

Supervisors: Derek Leinweber and Waseem Kamleh

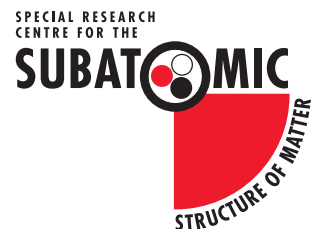
*Special Research Centre for the Subatomic Structure of Matter,  
Department of Physics, School of Physical Sciences  
University of Adelaide, Australia*

September 2016

A thesis submitted for the degree of Doctor of Philosophy  
of the University of Adelaide



THE UNIVERSITY  
*of* ADELAIDE



*This PhD thesis is dedicated to my parents,  
George and Kerry*

# Contents

<b>Abstract</b>	<b>xi</b>
<b>Acknowledgements</b>	<b>xiv</b>
<b>1 Introduction</b>	<b>1</b>
<b>2 Quantum Chromodynamics</b>	<b>3</b>
2.1 The Path Integral Formalism . . . . .	5
2.2 QCD on the Lattice . . . . .	7
2.2.1 Discretising QCD . . . . .	7
2.2.2 The Fermion Action on the Lattice . . . . .	8
2.2.3 Mean Field Improvement . . . . .	14
2.2.4 The Gauge Action on the Lattice . . . . .	15
<b>3 Spectroscopy in Lattice QCD</b>	<b>18</b>
3.1 Correlation Matrix Techniques . . . . .	18
3.2 Interpolating Operators . . . . .	20
3.3 Stochastic Propagator Techniques . . . . .	22
3.3.1 Smearing Stochastic Propagators . . . . .	24
3.4 Direct Correlator Evaluation . . . . .	25
3.5 $\gamma_5$ Hermiticity . . . . .	29
<b>4 The Nucleon Spectrum with Local Multi-hadron Operators</b>	<b>32</b>
4.1 Multi-Particle State Contributions . . . . .	34
4.2 Five-Quark Nucleon Interpolators . . . . .	35
4.3 Simulation Details . . . . .	36
4.4 Results . . . . .	37
4.4.1 Positive-Parity Results . . . . .	37
4.4.2 Negative-Parity Results . . . . .	43

<i>CONTENTS</i>	iii
4.5 Summary . . . . .	49
<b>5 Searching for Low-Lying States in the Roper Regime</b>	<b>50</b>
5.1 Five-Quark Interpolating Operators . . . . .	52
5.2 Simulation Details . . . . .	53
5.3 Results . . . . .	54
5.3.1 Correlation Matrix Construction . . . . .	54
5.3.2 Finite Volume Spectrum of States . . . . .	57
5.4 Summary . . . . .	59
<b>6 Non-Local Operators</b>	<b>61</b>
6.1 Noise Reduction Techniques . . . . .	62
6.1.1 Noise Minimisation Trick . . . . .	66
6.2 Simulation Details . . . . .	72
6.3 Five-Quark Operator Results . . . . .	74
6.4 Summary . . . . .	76
<b>7 Software Development</b>	<b>78</b>
7.1 Wick Contractions . . . . .	79
7.2 Correlator Size Reduction . . . . .	81
7.3 Calculations with Contracted Propagators . . . . .	83
7.4 Calculations Directly from Interpolators . . . . .	84
7.5 Future Directions . . . . .	91
<b>8 Conclusions</b>	<b>94</b>
8.1 Future Directions . . . . .	96
<b>A <math>\gamma</math>-Matrices</b>	<b>97</b>
A.1 Dirac Representation . . . . .	97
A.2 Pauli Representation . . . . .	99
<b>B Clebsch Gordan Coefficients</b>	<b>101</b>
<b>C One-End Trick</b>	<b>103</b>
<b>D Correlation Functions</b>	<b>105</b>
<b>Bibliography</b>	<b>119</b>

# List of Figures

2.1	A pictorial representation of the plaquette $U_{\mu\nu}(n)$ , the smallest possible closest loop on the lattice. . . . .	12
2.2	A pictorial representation of the term contributing to the clover $C_{\mu\nu}(n)$ . . . . .	13
3.1	Typical effective mass fits for positive-parity (left) and negative-parity (right) nucleon excitations. The left plot shows a fit to the first positive-parity excitation of a $4 \times 4$ correlation matrix. The fitted mass of 2.11(4) GeV provides $\chi^2/\text{dof} = 0.17$ . The plot on the right hand side shows a fit to the lowest-lying state in the negative-parity sector. It is sourced from a $6 \times 6$ correlation matrix. The fitted mass of 1.58(3) GeV corresponds to $\chi^2/\text{dof} = 0.87$ . We note that an earlier fit including $t = 20$ provides $\chi^2/\text{dof} = 1.22$ , reflecting the systematic drift in the effective mass at early times. . . . .	21
3.2	A comparison of correlators calculated with one stochastically estimated propagator (denoted “stochastic”) to those calculated with no stochastic propagators (denoted “standard”). Results are presented for the pion (left) and the ground state nucleon (right). . . . .	25
3.3	A comparison of pion effective mass plots produced using three different methods. The black data points are extracted from “standard method” correlator evaluation while the red and green points are obtained from the “direct method” of correlator evaluation, with and without $\gamma_5$ -Hermiticity respectively. . . . .	31
4.1	The Feynman diagrams considered following the introduction of five-quark interpolating fields to standard three-quark operators. . . . .	36

- 4.2 The positive-parity nucleon spectrum with various operator bases constructed with 35 and 200 sweeps of smearing. Horizontal solid lines are present to guide the eye and are drawn from the central value of the states in basis 4, while the dashed line marks the position of the non-interacting  $P$ -wave  $N\pi$  scattering threshold . . . 38
- 4.3 Eigenvector components corresponding to the low-lying positive-parity nucleon states. State 1 corresponds to the ground state, with states 2 and 3 corresponding to the first and second excited states respectively. The column numbers denote basis number while the minor  $x$  axis ticks correspond to the values of the variational parameter  $dt$  which runs from 1 through to 4.  $t_0 = 17$  has been used throughout. The subscripts 35 and 200 in the legend refer to the number of smearing sweeps applied. . . . . 39
- 4.4 Comparisons of eigenmasses to masses obtained from a projected correlator fit for low-lying states in the positive-parity nucleon channel. The column numbers denote basis number while the minor  $x$  axis ticks correspond to the values of the variational parameter  $dt = 1 \dots 4$ .  $t_0 = 17$  has been used throughout. The line denoting the extracted mass is set using basis 4 with  $dt = 3$ . . . . 41
- 4.5 A plot showing the eigenmasses for both states 2 and 3, illustrating the accidental degeneracy at  $dt = 2$ . . . . . 42
- 4.6 The negative-parity nucleon spectrum with various operator bases using 35 and 200 sweeps of smearing. Solid horizontal lines are present to guide the eye and are drawn from the central value of the states in basis 4, since this basis is the largest. The dashed line marks the position of the non-interacting  $S$ -wave  $N\pi$  scattering threshold. The variational parameters used herein are  $(t_0, dt) = (17, 3)$ . . . . . 44
- 4.7 Eigenvector components corresponding to State 0 which is in the region of the non-interacting  $S$ -wave  $N + \pi$  scattering threshold. The column numbers denote basis number while the minor  $x$  axis ticks correspond to the values of the variational parameter  $dt$  which runs from 1 through to 3.  $t_0 = 17$  has been used throughout. The subscripts 35 and 200 in the legend refer to the number of smearing sweeps applied. . . . . 45

4.8 Eigenvector components corresponding to low-lying negative-parity nucleon states. States 1 and 2 correspond to the two lowest-lying resonant states, while state 3 interestingly lies in the region of the  $P$ -wave scattering thresholds. The column numbers denote basis number while the minor  $x$  axis ticks correspond to the values of the variational parameter  $dt$  which runs from 1 through to 3.  $t_0 = 17$  has been used throughout. The subscripts 35 and 200 in the legend refer to the number of smearing sweeps applied. . . . . 46

4.9 Comparisons of eigenmasses to masses obtained from a projected correlator fit for state 0, which is in the region of the non-interacting  $S$ -wave  $N\pi$  scattering threshold. The column numbers denote basis number while the minor  $x$  axis ticks correspond to the values of the variational parameter  $dt = 1 \dots 3$ .  $t_0 = 17$  has been used throughout. The line denoting the extracted mass used has been set using basis 5 with  $dt = 3$ . . . . . 47

4.10 Comparisons of eigenmasses to masses obtained from a projected correlator fit for low lying states in the negative-parity nucleon channel. The column numbers denote basis number while the minor  $x$  axis ticks correspond to the values of the variational parameter  $dt = 1 \dots 3$ .  $t_0 = 17$  has been used throughout. The line denoting the extracted mass used has been set using basis 4 with  $dt = 3$ . . . . . 48

5.1 Correlation function ratios constructed to illustrate different superpositions of energy eigenstates in the correlators. The ratio is formed by dividing the correlator corresponding to each operator indicated in the legend by the correlation function formed from the  $\chi_1$  operator. Plots are presented at 35 (top left), 100 (top right) and 200 (bottom) sweeps of Gaussian smearing in the quark-propagator source and sink. For clarity of presentation, the  $t$  component of the ratio is sequentially offset. . . . . 55

5.2 Low-lying states observed for each of the correlation-matrix bases described in Table 5.1. For each interpolating field, two smearing levels of  $n_s = 35$  and  $n_s = 100$  are used in all cases. Dashed horizontal lines are present to guide the eye. They have been set by the central values from basis 1 in all cases except for the state  $\sim 2.1$  GeV, in which case it is drawn from basis 4. . . . . 58

- 6.1 Comparisons of pion effective mass plots with a point source using various dilution schemes. The source is inserted at timeslice 10. The black data points represent the effective mass extracted from a standard evaluation of the correlator. The red, blue and green mass plateaus are sourced from correlators evaluated from source vectors that possess full dilution in time-spin-colour (tsc), time-spin (ts) and time-colour (tc) indices respectively. Points in the top plot originate from the use of a single noise vector for both quark lines, while the bottom plot displays the results sourced from independent noise sources for each quark line. The  $x$ -component of the data points has been offset for clarity. . . . . 63
- 6.2 A plot of correlators  $\mathcal{G}$  for the nucleon operator  $\chi_1$ , calculated with an independent noise source for each quark line and full dilution in time and spin indices. Averaging of the correlator over all possible spatial source positions has been performed, and 150  $32^3 \times 64$  gauge configurations are utilised. The source is inserted at timeslice 16. Results are presented for four levels  $n_s = 0, 35, 100$  and 200 of Gaussian smearing at the source and the sink positions. Note that all estimates of the correlator drop below zero. Once the value of the correlator goes negative, further data points have not been plotted so as not to obscure the other values. The dashed horizontal line at zero is present to guide the eye. . . . . 65
- 6.3 A comparison of nucleon effective mass plots for a point source at  $t = 16$ . The black data points are calculated using standard point-to-all techniques, while the blue data points are calculated using the noise minimisation trick to stochastically estimate quark lines. In the stochastic case averaging over all possible spatial source positions has been performed. We utilise 150 of the  $32^3 \times 64$  gauge configurations used in chapter 5. Note that the effective mass plot for the stochastic estimation in the absence of the noise minimisation trick is not present as the value of the correlator becomes negative only 2 timeslices after the source insertion. . . . 71
- 6.4 The seven types of topologically distinct diagrams that must be evaluated in order to calculate the correlator as prescribed by Equation (6.15). The variables  $w$  and  $z$  correspond to spatial points at the source timeslice, while  $x$  and  $y$  correspond to spatial points at the sink time. . . . . 73



6.5	A plot of the ratio of the effective mass obtained from the momentum projected five-quark $\chi_{\pi N}$ operator to the sum of the effective masses obtained from standard nucleon and pion operators. The insertion of the point source occurs at timeslice 8, and 792 $16^3 \times 32$ gauge configurations have been used. . . . .	75
7.1	Nucleon quark tables for $u$ (left) and $d$ (right) quark sectors. The numbers correspond to the assigned quark number. . . . .	80
7.2	Nucleon quark tables for $u$ (left and centre) and $d$ (right) quark sectors post-permuting annihilation fields. These are the so-called “permutation tables”. . . . .	80
7.3	Nucleon quark tables after taking combinations of permutation tables. These are the so-called “contraction tables”. . . . .	80
7.4	The diagram corresponding to the pion correlation function. . . . .	89
7.5	The diagrams present when calculating the correlation function from the various five-quark meson-baryon creation and annihilation fields studied in this work. Note that while the different five-quark operators studied have different quark flavour structure, they all produce the diagrams shown. . . . .	90
7.6	A hypothetical diagram that <i>cfgen2</i> is able to calculate. Each quark line can take one of six flavours and be completely independent of any other quark line. Arbitrary numbers of free Lorentz or Dirac indices may be present on the correlator. Of course, this allows the independent momentum projection of each spatial source and sink point. The variables $(x, x', x'', x''')$ refer to pieces evaluated on the source timeslice, while the variables $(y, y', y'')$ are evaluated at the sink time. Naturally, given the computational challenges encountered throughout this research with five-quark operators, such a diagram would be prohibitively expensive to calculate with present computational resources. . . . .	92
B.1	<i>Clebsch-Gordan coefficients for the case <math>I' = 1, I'' = 1/2</math>.</i> Recall there is an implicit square root sign over the positive part of each table entry.	102

# List of Tables

3.1	The classification of various particles relevant to this work and their corresponding standard two- and three-quark interpolating fields. . . . .	21
4.1	Table of the various operators used in each basis. Two levels of $n_s = 35, 200$ sweeps of Gaussian smearing at the source and sink are used in the construction of each basis. The definition of the standard operators $\chi_1$ and $\chi_2$ can be found in Table 3.1, while $\chi_5$ and $\chi'_5$ are defined in Equation (4.5). . . . .	37
5.1	The interpolating fields used in constructing each correlation-matrix basis. Two levels of $n_s = 35, 100$ sweeps of Gaussian smearing at the source and sink are used in the construction of each basis. . .	56
6.1	A table showing the values of the three noise vectors, $\eta_A, \eta_B, \eta_C$ upon following our noise minimisation recipe. The three columns denoted ‘1’, ‘2’ and ‘3’ represent the three colour components of the noises. Here $d, e, f, g$ are random elements of $\mathcal{Z}_2$ while the ‘A’ in entry $\eta_C^1$ represents the fact that this assignment is an arbitrary $\mathcal{Z}_2$ element. Other entries are derived from Equations (6.4) and (6.6). . . . .	68

- 6.2 A table recording the number of timeslices after the source insertion,  $n_t$ , for which the nucleon correlator  $\mathcal{G}_N$  (corresponding to the operator  $\chi_1$ ) retains a positive sign for various methods of correlator evaluation. The “Standard Noise, dil = ts” column corresponds to the use of three independent stochastically estimated quark lines in the nucleon correlator with full dilution in time and spin indices, while the “Noise Min. Trick, dil = ts” column corresponds to the same recipe with the added implementation of the Noise Minimisation Trick encountered in Section 6.1.1. The final column refers to the nucleon correlator evaluated in the standard way with point-to-all propagators. 150  $32^3 \times 64$  gauge configurations were used, four different levels of  $n_s = 0, 35, 100$  and 200 sweeps of Gaussian smearing at the source and sink points were investigated and averaging over all possible spatial source positions has been performed for the stochastic estimates. . . . . 70

# Abstract

Since the inception of lattice QCD, significant effort has been invested into exploring hadronic spectra, both to shed light upon the nature and properties of various states, and to test the validity of the methodology itself. Critical challenges in this endeavour are the judicious selection of interpolating operators, and the choice of calculation paradigm within which these operators are utilised to extract observables.

In this thesis both of these challenges are addressed. Focusing on the topical nucleon sector, various local five-quark interpolating fields are introduced and spectroscopic calculations are performed with them. These local multi-hadron operators of interest give rise to diagrams that contain loop propagators that necessarily require a different calculation recipe. Stochastic estimation techniques are utilised to evaluate these propagation amplitudes, and a method to smear these propagators is developed.

The variational method for extracting hadronic excitations is then examined by producing spectra with a variety of operator bases. Fitting a single-state ansatz to the eigenstate-projected correlators is demonstrated to provide robust energies for the low-lying spectrum that are essentially invariant despite originating from qualitatively different bases.

In the negative-parity nucleon sector, the introduction of local five-quark operators permits the extraction of a state consistent with the  $S$ -wave  $\pi N$  scattering threshold, while in the positive-parity channel the excited state spectrum remains essentially unchanged under the addition of the local five-quark operators. Despite the use of multiple five-quark operators with qualitatively different quark,  $\gamma$ -matrix and parity structures, the overlap of local five-quark operators with five-quark scattering states is found to be low.

Non-local five-quark interpolating fields are then introduced, and stochastic noise minimisation techniques are developed in order to combat the computational difficulties introduced by these operators. Explicitly projecting momenta

onto single-hadron pieces of these non-local multi-hadron operators is known to provide significantly enhanced overlap with scattering states and as such we perform this projection enabling a presentation of a proof of principle calculation in the negative parity nucleon sector.

Furthermore, the calculation methodology and associated algorithms to evaluate correlators directly from  $n$ -quark operators are developed with a high degree of generality, forming the basis for a rich spectrum of future work in a wide variety of channels.

# Declaration

I certify that this work contains no material which has been accepted for the award of any other degree or diploma in my name, in any university or other tertiary institution and, to the best of my knowledge and belief, contains no material previously published or written by another person, except where due reference has been made in the text. In addition, I certify that no part of this work will, in the future, be used in a submission in my name, for any other degree or diploma in any university or other tertiary institution without the prior approval of the University of Adelaide and where applicable, any partner institution responsible for the joint award of this degree.

I give consent to this copy of my thesis when deposited in the University Library, being made available for loan and photocopying, subject to the provisions of the Copyright Act 1968. I acknowledge that copyright of published works contained within this thesis resides with the copyright holder(s) of those works.

I also give permission for the digital version of my thesis to be made available on the web, via the University's digital research repository, the Library Search and also through web search engines, unless permission has been granted by the University to restrict access for a period of time.

Adrian Leigh Kiratidis

# Acknowledgements

First and foremost, I'd like to thank my supervisors Derek Leinweber and Waseem Kamleh for their exceptional guidance, encouragement and patience throughout my PhD candidature as well as during my MPhil studies. During this time they have constantly made time for me in their busy schedules, always provided clear explanations and have seemed a never ending source of good ideas. Without them none of this would have been possible, so to that end I owe them greatly.

I'd also like to thank Derek for his financial support toward the end of this work, while I searched for particularly elusive bugs in my rather large piece of correlation function generation software, "cfgen".

The Adelaide CSSM lattice collaboration's software package "cola" was used extensively in this research, and I'd therefore like to mention it's author, Waseem Kamleh.

Throughout my years as a research student I've had the privilege of collaborating with many fellow researchers. In particular, conversations with, and ideas provided by Zhan-Wei, Finn and Tony Thomas have proved invaluable.

To the guys in the office that I've been lucky enough to share the PhD experience with, Daniel, Ben O., Alex, Finn, Sam, Ryan and everybody else, thanks for all the informative and thought provoking discussions, both on physics and non-physics related topics. They were of great help in both aiding my physics understanding and making the journey enjoyable. I also owe thanks to Silvana and Sharon in the CSSM office for everything that they do.

The PhD experience has also provided a wide range of opportunities to participate in activities not directly related to my research. Of particular note were the simulations Derek and I produced analysing the flight paths of various FIFA world cup soccer balls. These results will be published in a sports science journal shortly.

Finally I'd like to thank my family and friends for their support, encouragement and understanding. In particular I owe a special thanks to my parents, who

not only have supported and encouraged me over the course of my education but have greatly assisted in removing financial and logistical issues from my life for which I am greatly thankful. It is therefore to them, that this thesis is dedicated.